Characterization of the hysteresis cycle in a two-stage liquid-fueled swirled burner through numerical simulation

Benoit Cheneau, Aymeric Vié, Sebastien Ducruix

37th International Symposium on Combustion

Characterization of the hysteresis cycle in a two-stage liquid-fueled swirled burner through numerical simulation

B. Cheneau[1,2] A. Vié[1], S. Ducruix[1]

[1] *Laboratoire EM2C, CNRS, CentraleSupélec, Université Paris-Saclay, 3 rue Joliot Curie, 91192 Gif-sur-Yvette Cedex, FRANCE*

[2] *Safran Aircraft Engines Villaroche, Rond Point René Ravaud - Réau, 77550 Moissy-Cramayel, FRANCE*

CORRESPONDING AUTHOR:

Name: A. Vié

Address: Laboratoire EM2C,
CentraleSupelec,
3, rue Joliot Curie
91192 Gif-sur-Yvette Cedex, FRANCE

Phone: (+33)01 75 31 60 46

e-mail: aymeric.vie@centralesupelec.fr

COLLOQUIUM:

Colloquium: Gas turbines

PAPER LENGTH:

Abstract (Method 1) = **264 words**

Total Main Paper (Method 2) : **6194 words**

Main text
(6 full pages = 6 × 900 = 5400 words)
(1 half page = 450 words)
(0.763 half page = 344 words)

Characterization of the hysteresis cycle in a two-stage liquid-fueled swirled burner through numerical simulation

Benoit CHENEAU[a,b], Aymeric VIÉ[a,*], Sébastien DUCRUIX[a]

[a]*Laboratoire EM2C, CNRS, CentraleSupélec, Université Paris-Saclay, 3 rue Joliot Curie, 91192 Gif-sur-Yvette Cedex, FRANCE*
[b]*Safran Aircraft Engines Villaroche, Rond Point René Ravaud - Réau, 77550 Moissy-Cramayel, FRANCE*

Abstract

Lean Premixed Prevaporized combustors are today an interesting alternative to more classical configurations to reduce pollutant emissions. Still they may also give rise to strong flame dynamics and harmful combustion instabilities. In order to improve our control on such systems, multi-stage multi-injection burners offer additional degrees of freedom in the fuel distribution and thus in the combustion regime. The BIMER combustor has been expressly developed by EM2C to investigate this solution at a laboratory scale. It is composed of two swirling stages: the pilot stage, in which liquid fuel is injected through a pressure-swirl atomizer; and the multipoint stage, in which the fuel is injected through 10 holes in a jet-in-crossflow configuration. Successive experimental campaigns demonstrated the key-role played by fuel distribution in the two stages and clearly showed the existence of an hysteresis cycle: several flame stabilization archetypes can exist for the same fuel distribution, depending on the flow, spray and flame history. In-depth analysis through numerous experimental diagnostics permitted to elaborate several scenarii to explain this complex behavior. In the present study, large eddy simulations are carried out with the AVBP code to complement the experimental data in our understanding of the burner stabilization processes. Simulations from full pilot to full multipoint injections are performed, exhibiting the hysteresis cycle observed in the experiments. An original tri-stable point was also encountered for full pilot injection, with three possible flame shapes. This tri-stable point is investigated and the impact of fuel staging for a given flame shape is analyzed. The two bifurcations observed experimentally are finally presented and analyzed along with their inherent mechanisms.

Keywords: two-stage combustor, Large Eddy Simulation, bifurcation, turbulent spray flame

*Corresponding author:
Email address: aymeric.vie@centralesupelec.fr
(Aymeric VIÉ)

1. Introduction

By targeting a lean and homogeneous mixture of air and vaporized fuel, Lean Premixed Prevaporized (LPP) burners achieve cleaner and more efficient combustion compared to more classical configurations. They are however prone to extinction due to the very lean mixture, close to blow-off, that is targeted, to flashback and risks of strong thermo-acoustic instabilities [1]. To get additional control on the combustion process, a pilot injection is often used to generate a so-called pilot flame with the objective of preventing blow-off and extending the operation map [2]. The BIMER combustor has been expressly designed to study such systems at a laboratory scale [3, 4]. It is composed of two swirling stages: an outer stage in which the liquid fuel is injected through 10 equally spaced holes in a jet-in-crossflow configuration, the multipoint stage; and an inner stage in which the liquid fuel is injected through a pressure-swirl atomizer, the pilot stage [5]. The former stage, where most of the air is delivered, is dedicated to the LPP regime, while the latter is here to offer more control on the combustion.

In this burner, a key parameter is the staging factor, defined as the ratio between the liquid fuel mass flowrate in the pilot stage to the total liquid fuel mass flowrate. This is a potentially powerful tool to modify and locally control the fuel-to-air ratio, the flame shape and consequently the thermo-acoustic behavior of the combustor [6], without changing the power delivered by the engine, a critical point in most of the applications. It was shown in [3, 4] that modifying this parameter can lead to a bifurcation from a V-shaped to an M-shaped flame, resulting in an hysteresis cycle depending on the flow, spray and flame history. A third flame shape was also evidenced in [7, 8], the Tulip-shaped flame. While these flames are well-known flame archetypes in the context of swirling flows, and bi-stable flames were well-known in the literature [9–13], the possibility to trigger a specific shape by varying a single parameter was a novel aspect.

Successive experimental campaigns on the BIMER test bench made it possible to map the flame shapes as a function of the staging factor for given operating points at constant powers. Moreover, they also led to possible scenarii of transitions, thanks to detailed analysis of the spray and flow field. However, the detailed mechanisms leading to a given shape as well as a fine description of the impact of fuel staging on the flame characteristics is still of interest. To this purpose, Large Eddy Simulation (LES) will no doubt prove useful to access time- and space-resolved information. In the present work, the objective is thus to show how LES can complement the experimental studies and thus to improve our understanding of the operation of such a multi-staged burner.

In the following, the test bench is first described along with the associated numerical domain in Sec. 2. The simulation code and the numerical models are presented and commented in Sec. 3. Then, the targeted operating conditions as well as the numerical representation of the hysteresis cycle -as observed experimentally- are specified in Sec. 4. A qualitative description of the cycle is proposed in Sec. 5, relating flame shapes and bifurcations. An original tri-stable point was also encountered for full pilot injection, with three possible flame shapes. This tri-stable point for full pilot injection is detailed in Sec. 6, whereas the impact of fuel staging for a given flame shape is shown in Sec. 7. Finally, the scenarii for the two bifurcations are analyzed in Sec. 8.

2. The BIMER combustor

The BIMER test bench (Fig. 1) is a LPP combustor including a staged multipoint injection burner, based on an industrial geometry, and operating at atmospheric conditions [3, 4]. It is fed with preheated air at 473 K to enhance evaporation of dodecane, used as a surrogate of kerosene, and help in stabilizing combustion.

The injection device is composed of two swirling stages. The pilot stage is composed of 18 radial vanes and 15% of the total air mass flowrate is injected through this stage. A pressurized nozzle is integrated in the primary zone, on the injection device axis of symmetry, and creates a hollow cone of droplets with a 60° angle. The multipoint stage is composed of 20 radial vanes and delivers the remaining 85% of the total air mass flowrate. A multi-injection ring composed of 10 holes of 0.3 mm in diameter is used to inject fuel at high speed in a jet-in-crossflow configuration in this second stage. Multipoint injection is selected to enhance evaporation and mixing in order to prepare fresh gases for LPP combustion. Both stages are in a co-rotating configuration. They have been designed to create a strong recirculation zone thanks to the induced swirling motion. The geometrical swirl number is 1.0 for the multipoint stage and 0.6 for the pilot stage following [7, 14]. One of the key parameters of this study is the staging parameter α, defined as ratio between the mass flowrate of fuel injected in the pilot stage to the total mass flowrate of fuel [5].

The injection device is placed in a cylindrical plenum (see Fig. 1). The combustion chamber has a rectangular cross-section (150×150 mm^2) and its length is 500 mm. Two silica windows are located on lateral sides for optical access. The chamber top, bottom and entrance plane walls are water-cooled to ensure thermal regulation for

long duration tests. Numerous diagnostics are available experimentally for the gas phase and the spray [3, 4, 7].

The operating point of the present work is the one studied in [3, 4]. It corresponds to a global air mass flowrate of 53 g.s^{-1} and a global mass fuel rate of 1.94 g.s^{-1}. The global equivalence ratio is around 0.54, and the power developed is approximately 85 kW. It is important to note that for various practical reasons detailed in [3, 4], the range of staging factor available experimentally is bounded: $\alpha \in [20; 60]\%$. As it will be shown below, this is not the case numerically.

The ignition sequence is started with pure pilot injection, but for a lower mass flowrate and a higher equivalence ratio, for safety reasons. This will not be the case on the simulation side, where the nominal operating point can be used for ignition (pure pilot case also).

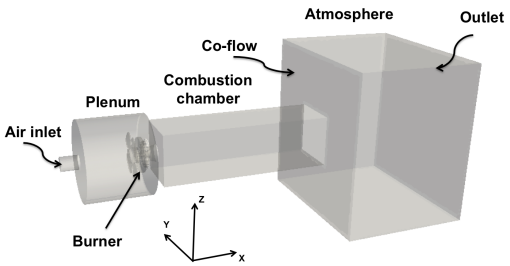

Figure 1: BIMER setup, numerical domain. Flow from left to right.

3. Modeling and numerical set-up

The present configuration is simulated using LES with the 3D unstructured AVBP solver developed by CERFACS and IFPEN [15]. The two-phase flow formalism detailed in [16] is considered here. For the gaseous phase, the multi-species Navier-Stokes equations for reacting flows are computed. Unity Lewis number is assumed for all species and the BFER reduced mechanism [17], which accounts for 5 species and 2 reactions, is used. Sub-grid scales are modeled with the Wall-adapting Local Eddy-Viscosity (WALE) model [18], to ensure a satisfactory behavior for the near wall flow. The combustion is modeled using the Dynamic Thickened Flame LES model [19] with a dynamic thickening of the flame front in order to guarantee a good representation of the reaction zone on the mesh. The thickening factor depends on the mesh resolution and the filtered wrinkling surface of the flame is corrected by an efficiency function [20]. The liquid phase is represented using a LES monodisperse-monokinetic Eulerian formalism, as in [21]. Even if developments have been made to handle polydispersity [22], a monodisperse model (i.e. the spray is described by one droplet size at each time and location) has been used to limit the computational cost of the whole simulation campaign. This monodisperse assumption is known to possibly lead to underestimated spray opening in swirled conditions [22]. However, it has been shown in [23] that polydisperse laminar spray flames can be well-reproduced with a monodisperse spray using the Sauter Mean Diameter of the initial distribution, a strategy that is also chosen in the present study.

The domain (Fig. 1) is numerically represented with an unstructured mesh of 10 million tetrahedra. A mesh refinement up to 40 million cells has been carried out to guarantee that the solution is not dependent on the mesh (not shown here). The domain starts a few centimeters before the cylindrical plenum entrance and ends with an additional volume mimicking the room atmosphere, in order to avoid non-physical interactions between the combustion chamber and the domain outlet. A co-flow is added to the atmosphere to prevent unwanted recirculation. To simulate the set of equations, a Two-Step Taylor Galerkin finite element scheme [24], 3rd order time and space, is used. Gaseous inlet and outlet boundary conditions are treated using the Navier-Stokes Characteristic Boundary Conditions framework [25]. A no-slip condition is used on walls for the gas, while droplets slip freely on them. All walls are considered adiabatic, except top, bottom and entrance plane walls of the combustion chamber that are water-cooled in the experiment. For the latter, a constant isothermal condition is tuned to obtain the same power extraction as in the experiments. For the liquid phase, the pilot injection is modeled using the FIMUR model (Fuel Injection Model by Upstream Reconstruction, [16]) with droplets of 40 μm, while the multipoint injection is represented by a Neumann boundary condition with imposed flowrate and with droplets of 20 μm. The surface of the 10 multipoint holes is numerically increased by a factor five on the diameter in order to alleviate the constraint on the mesh smaller cell. The associated inlet momentum is chosen in order to avoid direct impact of the droplets on the wall facing the injection hole, as observed experimentally.

4. Operating conditions and numerical cycle

The two liquid injection types were tested in a preliminary study [26]. While inaccessible experimentally (see Sec. 2), this first work validated the injection procedures and highlighted their dramatic influence on the flame stabilization process. Indeed, when fuel is solely

injected through the multipoint stage, evaporation and mixing are fast and the mixture that enters the combustion chamber is quite well-premixed. The flame then takes an M-shape, mainly controlled by the large central and outer recirculation zones (CRZ and ORZ, respectively) associated with the highly swirling chamber flow and in which trapped burnt gases guarantee permanent ignition of the fresh mixture entering the chamber. The situation is much more complex when fuel is solely injected through the pilot nozzle. Due to the large amount of liquid fuel present in the pilot zone, premixing is not achieved and the flame must stabilize itself in a hybrid combustion regime. This is only possible thanks to a complicated mixing process in this region, where hot evaporated fuel is trapped in front of the nozzle and oxygen is mainly coming from the large CRZ. In that case, the flame takes a Tulip-shape, with a stabilization point inside the injection device. Details can be found in [26].

Besides these pure pilot ($\alpha = 100\%$) and multipoint ($\alpha = 0\%$) cases, the staging factors $\alpha = 60, 35$ and 20%, accessible experimentally were simulated. As history plays a key role, the following protocol, faithful to the experimental one, was implemented (Fig. 2). After a pure pilot ignition ($\alpha = 100\%$), α is decreased by successive steps at 60, 35 et 20% towards zero (red line and arrows on Fig. 2). To end the cycle, α is increased back to $\alpha = 100\%$, starting from (1) $\alpha = 0\%$ (blue line and arrows at the top of Fig. 2) and (2) $\alpha = 60\%$ (blue line and arrow in the middle of Fig. 2). In order to be

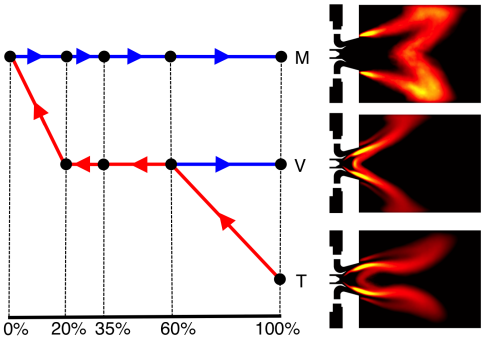

Figure 2: Schematic description of the cycle followed numerically. T stands for Tulip shape, V for V shape and M for M shape. Arrows indicate the direction of variation of α. Stabilized mean flame archetypes are shown: M-flame (top), V-flame (center) and Tulip flame (bottom).

more precise, and to differentiate the cases obtained at identical staging factors, but from increasing or decreasing variations, four steps and the symbols $\nearrow$ and $\searrow$ are introduced in the following:

1. $\alpha^{\text{ign}}_{100}$ is the ignition case.
2. $\alpha^{\searrow}_{60}$, $\alpha^{\searrow}_{35}$, $\alpha^{\searrow}_{20}$ and $\alpha^{\searrow}_{00}$ are obtained by decreasing α starting from the $\alpha^{\text{ign}}_{100}$ case.
3. $\alpha^{\nearrow}_{20}$, $\alpha^{\nearrow}_{35}$, $\alpha^{\nearrow}_{60}$ and $\alpha^{\nearrow}_{100}$ are obtained by increasing α back starting from the above $\alpha^{\searrow}_{00}$ case.
4. $\alpha^{\nearrow}_{100^{\text{bis}}}$ is obtained by increasing α back, but starting from the above $\alpha^{\searrow}_{60}$ case this time.

Variations of α are expressed in percentage point (pp) of pilot injection. A variation rate of 1 ms for 1 pp was used for α. This time scale corresponds to the time taken by the injected fuel to reach the flame tip. Each staging factor variation is followed by a stabilization period of 20 ms, after which the main physical parameters (kinetic energy, pressure, heat release, temperature, etc.) are checked for convergence. Finally the average flow field is recorded over an additional time of 80 ms. The convergence of the simulations for each staging factor is generally very fast. Indeed, initial and final states are the same in the sense of equilibrium.

5. Full cycle description

Following this protocol, eleven simulations have been carried out leading to several changes of the flame shape that are also visible on Fig. 2 and now summarized following the four steps introduced in Sec. 4:

1. We start from the Tulip flame obtained by ignition at the full pilot injection ($\alpha^{\text{ign}}_{100}$) [26];
2. α is decreased down to $\alpha^{\searrow}_{60}$. A first bifurcation occurs leading to a V-flame. The flame keeps a V-shape when stabilizing $\alpha^{\searrow}_{35}$ and $\alpha^{\searrow}_{20}$. Then, going down to $\alpha^{\searrow}_{00}$, a second bifurcation occurs, leading to an M-shape;
3. Increasing α back, this M-shape is preserved up to full pilot injection: $\alpha^{\nearrow}_{20}$, $\alpha^{\nearrow}_{35}$, $\alpha^{\nearrow}_{60}$ and $\alpha^{\nearrow}_{100}$) show very similar flame shapes and structures;
4. An additional point has been simulated from the V-flame at $\alpha^{\searrow}_{60}$: increasing α up to $\alpha^{\nearrow}_{100^{\text{bis}}}$, the flame keeps a V-shape.

To sum-up, two bifurcations occur during the whole cycle, leading to a remarkable tri-stable point for full pilot injection: $\alpha^{\text{ign}}_{100}$, $\alpha^{\nearrow}_{100}$ and $\alpha^{\nearrow}_{100^{\text{bis}}}$. Moreover, two flame shapes are observed for a wide range of staging factors (V and M). At this point it is important to mention that the numerical study of bifurcations cannot exactly follow the experimental protocol for obvious reasons of computational cost. Indeed, simulated physical times are one or two order magnitudes smaller than in the experiments. Thus, the conclusions concerning the persistence of a given flame archetype should be handled

with care, as transitions may occur for latter times due to different degrees of randomness. Still, the very good agreement between the numerical simulations and the experiments for intermediate staging and the fact that the Tulip flame shape has been evidenced experimentally for a lower power in [8] give us a great confidence in the flame archetypes found for full pilot injection, even if no experiment is available. In the following, we will first compare the three flame shapes obtained for full pilot injection. Then we will analyze the impact of fuel staging for a given flame shape. Finally, we will investigate the two bifurcations that were observed here.

6. Tri-stable point for full pilot injection

As demonstrated in Sec. 5, three flame stabilization scenarii are obtained for the same injection conditions. The three flames are presented in Fig. 4 and their -common or distinct- features are described below. The M-flame is anchored at the diffuser exit, in the ORZ, and crosses the CRZ in its narrowing region. The Tulip flame shares with the M-flame the same aerodynamical features, although completely surrounding the CRZ. Unlike the M-flame, it is anchored at the pilot stage exit. The V-flame shares with the Tulip flame the same stabilization and anchorage process but shows different aerodynamical features: the CRZ is widely open without any narrowing, and the flame reaches the side walls.

Apart from the flame shape, an interesting aspect concerns the combustion regime(s) encountered in each flame, which can be identified through the reactive Takeno index Ta, as in [27], which discriminate premixed (Ta $>$ 0) and diffusion reaction zones (Ta $<$ 0). In Fig. 4, the Takeno index is presented in the physical space (left). Scatterplots of the temperature versus the mixture fraction based on carbon atoms are also shown (right). The V- and Tulip flames share a similar flame structure: they both reach the equilibrium in the diffusion-like zone in the burner diffuser, while premixed regions are visible at the corners and CRZ borders. The main difference comes from the potential overlap between the high temperature region and the spray region, due to the proximity of the central diffusion flame to the injection region. On the other side, the M-flame is essentially burning in a premixed regime, thus achieving the expected LPP regime. The diffusion-like zones are mainly due to a bias of the Takeno index that can lead to "diffusion artifact" in the case of premixed spray flames.

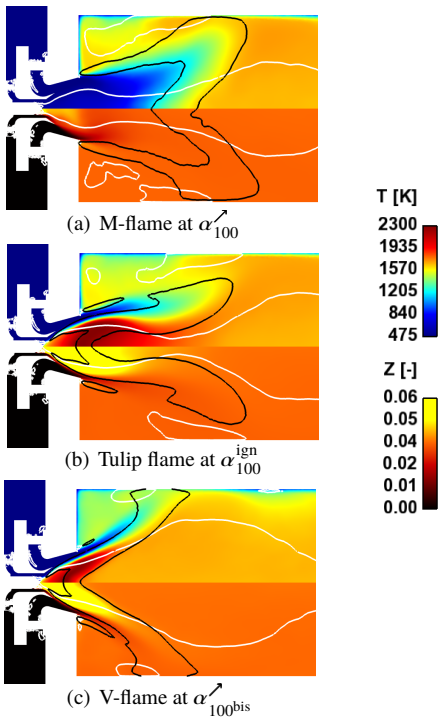

(a) M-flame at $\alpha^{\nearrow}_{100}$

(b) Tulip flame at $\alpha^{\text{ign}}_{100}$

(c) V-flame at $\alpha^{\nearrow}_{100^{\text{bis}}}$

Figure 3: Cut plane of the time-averaged temperature and mixture fraction fields for the three flame archetypes. Isocontours of null axial velocity (white line) and heat release rate at 5.10^6 W.m^{-3} (black line).

7. Impact of fuel staging

The focus is now on two given flame shapes (M and V). The impact of fuel staging on their inner structure -mixing and combustion regime- is investigated. As schematically shown in Fig. 2, when increasing α from 0 to 100% (resp. 60 to 100%), the overall M- (resp. V-) shape of the flame is not affected by fuel staging (not shown here). Section 6 already described qualitatively the global flame structure. This kind of tridimensional analysis could not be carried out experimentally, and simulations clearly bring a key asset to the understanding of this type of burner behavior.

The first variable of interest is the mixture fraction distribution in the flame region (Fig. 5). Since the objective of the LPP burner is to ensure a lean homogeneous combustion, this metric is important as it quantifies how far from the expected scenario the flame burns. Figure 5 shows that both flames are mainly burning at the global mixture fraction, fulfilling the objectives of both flame archetypes. However, the V-flame generates richer mixtures and thus richer combustion because of the flame interaction with the spray at the pilot nozzle exit. Observing the two extreme staging for both flame archetypes, it is also noticeable that the overall mixture

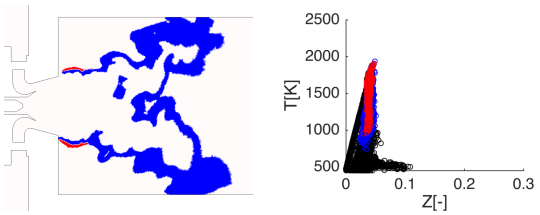

(a) M-flame at $\alpha^{\nearrow}_{100}$

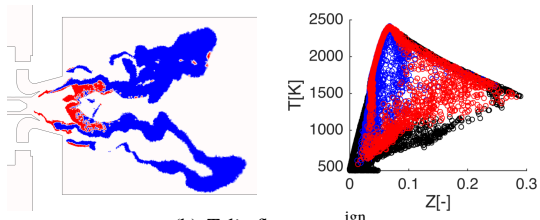

(b) Tulip flame at $\alpha^{\text{ign}}_{100}$

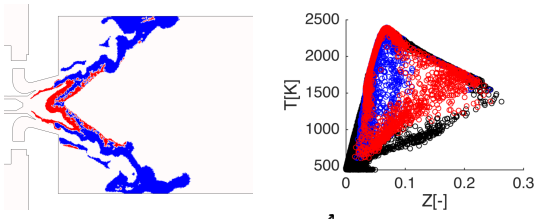

(c) V-flame at $\alpha^{\nearrow}_{100^{\text{bis}}}$

Figure 4: Instantaneous cut plane of the Takeno index in the reaction zone (left) and Scatterplot of the temperature versus mixture fraction colored by the Takeno index when the heat release rate is higher than 10^6 W.m^{-3} (right) for the three flames for full pilot injection. Premixed regime in blue and diffusion regime in red.

fraction distribution is not affected by the change in α, the only impact being on the standard deviation.

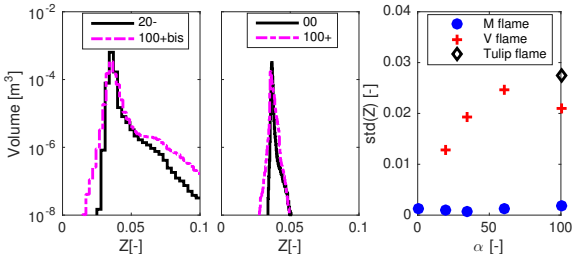

Figure 5: Mixture fraction distribution for V (left) and M (center) flames for minimum and maximum staging factor that stabilizes these flames. Standard deviation of the mixture fraction as a function of the staging factor for all flame shapes. Distributions are taken in the flame region where the heat release is higher than 10^6 W.m^{-3}.

To identify the combustion regimes, we define two indices: the Diffusion Index (I_{diff}) that evaluates the ratio between flame volume in diffusion regime to the overall flame volume, and the Gaseous Combustion Index (I_{gas}) that estimates the ratio between flame volume in pure gaseous combustion to the overall flame volume:

$$I_{\text{diff}} = \frac{V_{\text{Ta}<0,\dot{\omega}>10^6}}{V_{\dot{\omega}>10^6}}, \quad I_{\text{gas}} = \frac{V_{\alpha_l<10^{-6},\dot{\omega}>10^6}}{V_{\dot{\omega}>10^6}} \qquad (1)$$

where V is the volume of the zone fulfilling the conditions in its subscript. The two indices are presented in Fig. 6. While the M-flame mainly burns in a premixed regime, there are still more occurrences of diffusion-like regime as we increase α. The same trend can be found for the gaseous character of the flame, increasing α generating more and more overlapping regions between the spray and the reaction zones.

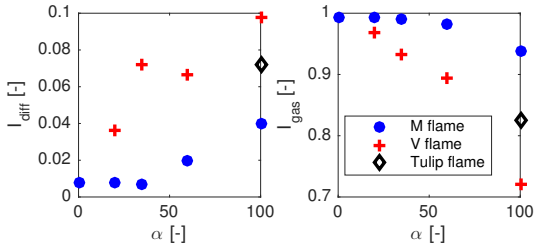

Figure 6: Diffusion (left) and Gaseous combustion indices (right) as a function of the staging factor.

8. Flame shape bifurcations

Studying the flame shape transitions experimentally is possible [7, 8], but remains a difficult task due to the lack of information. As two transitions could be obtained by simulations, the physical mechanisms leading to them are investigated. For both transitions, we first describe their time evolution and we then propose possible mechanisms and scenarii.

8.1. Tulip-to-V transition

Starting from a stable Tulip flame (Fig. 7a), α is decreased. It is first observed that the rich flame at the divergent exit moves inside the divergent because of the decrease of the local mixture fraction (b). The length (and thus volume) of the flame stabilized around the CRZ is increased, since more fuel directly goes into this region thanks to the multipoint injection. Secondly, the flow adapts itself to this modification by opening the CRZ (c). This opening is a slow and progressive event that ends to the final V-flame with the fully open CRZ (d). The transition is similar to what can be observed when increasing the swirl number: starting from a narrow CRZ, the swirl increase leads to a wide opening of the CRZ. In the spirit of this scenario, we thus expect

this transition to be due to the local modification of the aerodynamical features of the flow at the divergent exit. Thus, we do not observe a modification of the flame structure, but only a modification of the aerodynamics because of the flame displacement in the divergent.

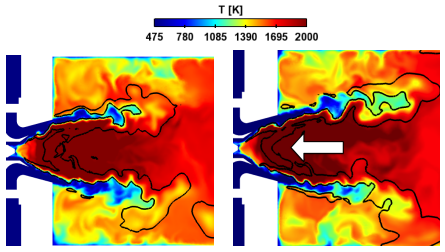

(a) Tulip flame at $\alpha^{\text{ign}}_{100}$ (b) Rich flame displacement

(c) Opening of the CRZ (d) Final V-flame at $\alpha_{60}^{\searrow}$

Figure 7: Tulip-to-V flame transition: temperature field cut plane and isoline of heat release rate at $\dot{\omega} = 50$ MW.m^{-3} (black) at main events.

8.2. *V-to-M transition*

Compared to the Tulip-to-V transition, the V-to-M transition is more complex, as visible in Fig. 8. Starting from the V-flame at $\alpha = 20$ %, the interruption of the pilot injection leads to the flame extinction at the injector exit and to the so-called V* flame. This V* flame is no longer attached to the pilot injector but it keeps the same stabilization between the CRZ and the ORZ. The flame persists in this meta-stable state during nearly 100 ms after the end of the extinction ramp of the pilot injection. Meanwhile, we observed several vortices that are affecting the inner flame front (c) without modifying the flame structure. However, when this perturbation is large enough, it leads to the merging of the inner flame inside the recirculation zone (d). The resulting flame front propagates back to the pilot injection (e) and then extinguishes as no fuel is available in this zone anymore, to finally lead to the M-flame. This transition seems to be due to a random event, i.e. a vortical perturbation large enough to merge the inner surface of the flame inside the CRZ. This random event leads to a dramatic modification of both the flame and the aerodynamics, finally leading to the stable M-flame state. The precise features of this random event are not known yet and it is left for future work.

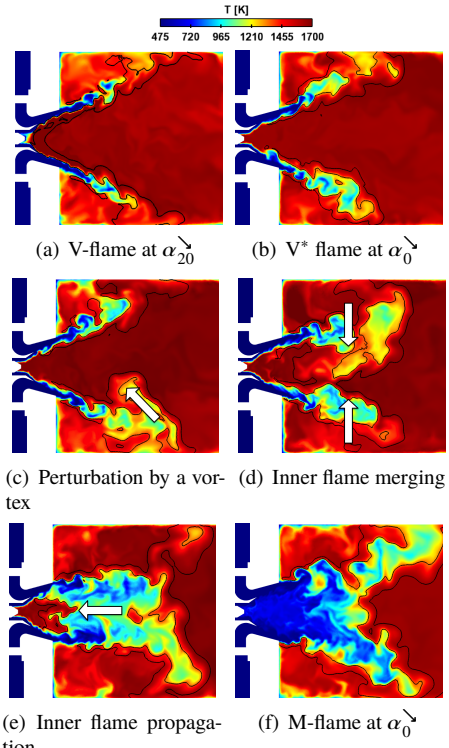

(a) V-flame at $\alpha_{20}^{\searrow}$ (b) V* flame at $\alpha_{0}^{\searrow}$

(c) Perturbation by a vortex (d) Inner flame merging

(e) Inner flame propagation (f) M-flame at $\alpha_{0}^{\searrow}$

Figure 8: V-to-M flame transition: temperature field cut plane and isoline of heat release rate at $\dot{\omega} = 50$ MW.m^{-3} (black) at main events.

9. Conclusion

The influence of fuel staging on the flame structure of a two-staged multipoint burner has been investigated to improve the understanding of this burner behavior. In the scope of completing experimental studies, simulation were conducted over the whole range of staging factor, from fully pilot to fully multipoint injection. The hysteresis phenomenon found in the experiments is retrieved. For $\alpha \in [20, 65]$ % two flames are generated depending on the flow history: a M- and a V-flame. Moreover, for full pilot injection an additional Tulip flame can also be found, resulting in a tri-stable point. Two bifurcations of flame structure are also detected: the transition from Tulip to V-flame, and from V- to M-flame.

The tri-stable point at $\alpha = 100$ % is then analyzed, to identify the differences and similarities between the encountered flame archetypes. First, M- and Tulip flames share the same aerodynamics, with a contracted CRZ, whereas the V-flame CRZ is widely open. Addition-

ally, Tulip and V-flames share the same flame structure with highly rich regions burning in a diffusion-like regime, while the M-flame mainly burns in a lean premixed regime, as targeted by this LPP combustor. To this end and because the Tulip flame archetype does not reach the LPP regime and promotes sound pressure levels as high as the M-flame one (not shown here), full pilot injection should be avoided.

As intermediate staging factors have proved to be useful for operationally reasons, we further investigated the impact of fuel staging on flame shape and structure. The reaction region has been characterized regarding the quality of the mixing and the combustion regime. As expected the V and Tulip flames exhibit highly non-homogeneous mixtures with rich regions, promoting diffusion-like combustion regime with a strong interaction with the spray, this tendency being enhanced as we increased the staging factor. We also clearly evidenced an optimal region where diffusion regimes are avoided and for which both V- and M- flames are close to the minimal diffusion index, here for $\alpha \leq 35\%$.

Finally, the two bifurcations are investigated, to highlight the events of the transitions. The Tulip-to-V flame is shown to be driven by a smooth adaptation of the flow field to the new conditions in the divergent. On the contrary, the V-to-M transition is driven by a "catastrophic" event that collapse the inner flame inside the CRZ. A perspective of this work is thus to identify the reasons of the occurrence of this event which was not observed for higher staging factors. Looking at the staging factor as a control parameter, it is interesting to use these transitions in order to avoid the Tulip flame archetype and directly reach an LPP regime by stabilizing an M-flame.

Acknowledgments

The support of Safran Aircraft Engine and ANRT for the PhD grant of B. Cheneau is gratefully acknowledged. This work was granted access to the HPC resources of CINES under the allocation 20162b0164 made available by GENCI (Grand Equipement National de Calcul Intensif). The authors would also like to thank CERFACS and IFPEN for sharing the AVBP code, and L. Zimmer and A. Renaud for fruitful discussions.

References

[1] S. Ducruix, T. Schuller, D. Durox, S. Candel, Journal of Propulsion and Power 19 (2003) 722–734.
[2] P. Albrecht, S. Bade, A. Lacarelle, C. O. Paschereit, E. Gutmark, J. Eng. Gas Turb. and Power 132 (2010) 041501–8.
[3] T. Providakis, L. Zimmer, P. Scouflaire, S. Ducruix, Comptes Rendus Mecanique 341 (2013) 4–14.
[4] T. Providakis, L. Zimmer, P. Scouflaire, S. Ducruix, Journal of Engineering for Gas Turbines and Power 134 (2012) 111503–8.
[5] S. Barbosa, P. Scouflaire, S. Ducruix, Proceedings of the Combustion Institute 32 (2009) 2965–2972.
[6] D. Durox, T. Schuller, N. Noiray, S. Candel, Proceedings of the Combustion Institute 32 (2009) 1391–1398.
[7] A. Renaud, S. Ducruix, P. Scouflaire, L. Zimmer, Proceedings of the Combustion Institute 35 (2015) 3365–3372.
[8] A. Renaud, S. Ducruix, L. Zimmer, Proceedings of the Combustion Institute (2017) 3899–3906.
[9] Y. Huang, V. Yang, Prog. Energy Comb. Sci. 35 (2009) 293–364.
[10] S. Hermeth, G. Staffelbach, L. Y. M. Gicquel, V. Anisimov, C. Cirigliano, T. Poinsot, Combust. Flame 161 (2013) 184 – 196.
[11] D. Durox, K. Prieur, T. Schuller, S. Candel, J. Eng. Gas Turb. and Power 138 (2015) 101504.
[12] K. Oberleithner, M. Stöhr, S. H. Im, C. M. Arndt, A. Steinberg, Combust. Flame 162 (2015) 3100–3114.
[13] M. Stöhr, K. Oberleithner, M. Sieber, Z. Yin, W. Meier, J. Eng. Gas Turb. and Power 140 (2018) 011503.
[14] D. Galley, S. Ducruix, F. Lacas, D. Veynante, Combustion and Flame 158 (2011) 155–171.
[15] P. Wolf, R. Balakrishnan, G. Staffelbach, L. Gicquel, T. Poinsot, Flow, Turbulence and Combustion 88 (2012) 191–206.
[16] M. Sanjosé, J.-M. Senoner, F. Jaegle, B. Cuenot, S. Moreau, T. Poinsot, International Journal of Multiphase Flow 37 (2011) 514–529.
[17] B. Franzelli, E. Riber, M. Sanjosé, T. Poinsot, Combustion and Flame 157 (2010) 1364 – 1373.
[18] F. Nicoud, F. Ducros, Flow, Turbulence and Combustion 62 (1999) 183–200.
[19] O. Colin, F. Ducros, D. Veynante, T. Poinsot, Physics of Fluids 12 (2000) 1843–1863.
[20] F. Charlette, C. Meneveau, D. Veynante, Combustion and Flame 131 (2002) 181 – 197.
[21] B. Franzelli, A. Vié, M. Boileau, B. Fiorina, N. Darabiha, Flow, Turb. and Comb. 98 (2017) 633–661.
[22] A. Vié, S. Jay, B. Cuenot, M. Massot, Flow, Turbulence and Combustion (2013) 1–37.
[23] D. R. Ballal, A. H. Lefebvre, Proc. Combust. Inst. 18 (1981) 321–327.
[24] O. Colin, M. Rudgyard, Journal of Computational Physics 162 (2000) 338 – 371.
[25] T. Poinsot, S. Lele, Journal of Computational Physics 101(1) (1992) 104–129.
[26] B. Cheneau, A. Vié, S. Ducruix, ASME Turbo Expo 2015 GT2015-56680 (2015).
[27] G. Hannebique, P. Sierra, E. Riber, B. Cuenot, Flow, Turbulence and Combustion (2012) 1–21.